

Following moist intrusions into the Arctic using SHEBA observations in a Lagrangian perspective

Syed Mubashshir Ali^{1,2,3} | Felix Pithan¹

¹Alfred Wegener Institute, Helmholtz Centre for Polar and Marine Research, Bremerhaven, Germany

²Institute of Environmental Physics, University of Bremen, Bremen, Germany

³Institute of Geography and Oeschger Centre for Climate Change Research, University of Bern, Bern, Switzerland

Correspondence

Syed Mubashshir Ali, Institute of Geography, University of Bern, Haldenstrasse 12, 3012, Bern, Switzerland
Email: mubashshir.ali@giub.unibe.ch

Funding information

The Helmholtz Association (HGF), Grant Reference Number PD-300

Warm and moist air masses are transported into the Arctic from lower latitudes throughout the year. Especially in winter, such moist intrusions can trigger cloud formation and surface warming. While a typical cloudy state of the Arctic winter boundary layer has been linked to the advection of moist air masses, direct observations of the transformation from moist mid-latitude to dry Arctic air are lacking. Here, we have used observations from the Surface Heat Budget of the Arctic Ocean (SHEBA) project to compile Eulerian observations along the trajectories of warm and cold air masses in a Lagrangian sense, showing the cooling and drying of air masses over sea ice and moistening over the open ocean. Air masses originating mostly over open water generate cloudy conditions over the observation site, whereas air masses originating over continents or sea ice generate radiatively clear conditions. We recommend using our case studies for modelling work and the method of linking expeditions to station soundings via back-trajectories for future campaigns.

KEYWORDS

air mass transformation, moist air intrusion, cloudy state, Arctic, Polar atmosphere, SHEBA

Abbreviations: MI, Moist Intrusions; SHEBA, Surface Heat Budget of the Arctic; MOSAIC, The Multidisciplinary drifting Observatory for the Study of Arctic Climate

This article has been accepted for publication and undergone full peer review but has not been through the copyediting, typesetting, pagination and proofreading process which may lead to differences between this version and the Version of Record. Please cite this article as doi: 10.1002/qj.3859

1 | INTRODUCTION

The Arctic has a sparse observational coverage compared to lower latitudes. Its hostile climate and the dynamical sea ice pose operational challenges for regular in-situ observations. Satellite remote sensing is often limited by geographical coverage issues, low surface contrasts, the lack of daylight during polar night or strong cloudiness. The lack of observations is a major challenge in understanding the polar key processes and thus, predicting Arctic weather and climate which is undergoing an amplified change in a warming world (Hansen et al., 2010). Improving Arctic forecasts also has the potential to contribute to more skilful medium-range and sub-seasonal forecast for the Northern Hemisphere mid-latitudes (Jung et al., 2014). To address that, collaborative international efforts are underway to advance Polar prediction capabilities (Jung et al., 2016; Dethloff et al., 2016).

The Surface Heat Budget of the Arctic (SHEBA) (Persson et al., 2002) and the Norwegian Young Sea Ice (N-ICE2015) expeditions (Granskog et al., 2016) have shown that the wintertime Arctic boundary layer is characterized by a bi-modal distribution between a radiatively clear and an opaquely cloudy state (Stramler et al., 2011; Morrison et al., 2012; Graham et al., 2017). This bi-modality is also observed in the time series from the ARM site in Utqiagvik, (formerly known as Barrow), Alaska for the boreal winter (Pithan et al., 2014, Figure 10). The two states have different net surface longwave radiation (NetLW) as the clear state is characterised by strong longwave cooling (NetLW $\sim -40W m^{-2}$) under clear skies or ice clouds and the cloudy state with little to no surface cooling (NetLW $\sim 0W m^{-2}$) under low-level mixed-phase clouds (Stramler et al., 2011; Morrison et al., 2012; Pithan et al., 2014). These states also exhibit different boundary layer temperature profiles with the clear state showing surface-based inversions and the cloudy state often showing an elevated and weaker inversion (Stramler et al., 2011; Cohen et al., 2017). Moreover, the clear state has a dry atmospheric profile whereas the cloudy state profile shows a high moisture content (Stramler et al., 2011). The enhanced downward longwave emissions due to the presence of clouds and moisture substantially impact the wintertime surface heat budget of the Arctic (Stramler et al., 2011) and knowing the frequency of these states is crucial to determine the surface energy budget and thus winter sea ice thickness (Morrison et al., 2012).

During wintertime, once the Arctic ocean freezes, it has no major local moisture sources. Fluxes from open leads can be large locally but have a small contribution to the overall heat and moisture budget (Walter et al., 1995; Serreze et al., 2007). A large fraction of the water vapour in the Arctic wintertime troposphere is advected in events of warm and moist air-mass transport from lower latitudes. These events are referred to as moist intrusions and take place in the form of pulses throughout the year (Doyle et al., 2011). Woods and Caballero (2016) showed an increase in moist intrusions originating in the North Atlantic and North Pacific during wintertime. Moist intrusions are usually triggered by an anticyclonic-blocking like feature to the east and a low-pressure system to the west (Woods et al., 2013; Pithan et al., 2018). Recently, moist intrusions have also been linked to Rossby wave breaking events (Liu and Barnes, 2015).

Moist intrusions cause strong downward longwave radiation due to a high localised concentration of water vapour which can lead to anomalous surface warming over land or sea ice (Kapsch et al., 2013; Pithan et al., 2014; Park et al., 2015; Woods and Caballero, 2016; Pithan et al., 2016; Johansson et al., 2017). During 2003-2014, moist intrusions from the North Atlantic and Pacific caused local surface temperature anomalies of up to 8K and 10 K respectively. These warm anomalies can have further implications for sea ice recovery during winter and may cause a premature spring melt (Kapsch et al., 2013; Mortin et al., 2016; Kapsch et al., 2016). Nearly half of the sea ice concentration decline between 1979 and 2011 over the Barents-Kara Seas and Baffin Bay has been attributed to enhanced downward infrared radiation driven by such moist intrusions (Park et al., 2015). These events have also been associated with summer Greenland ice sheet melt in July 2012 (Bennartz et al., 2013).

Several studies have investigated air-mass transformation occurring during the advection of air masses from low latitudes into the Arctic (Wexler, 1936; Curry, 1983; Emanuel, 2008; Pithan et al., 2014). The idealised single-column

model experiments have shown that radiative cooling is an important process driving the transformation of these air masses (Curry, 1983; Emanuel, 2008; Pithan et al., 2014). However, the radiative cooling is very sensitive to the moisture content of the air mass and the presence of cloud condensate. Pithan et al. (2014, Figure 6) showed that as the warm air masses are advected polewards, the rapid cooling leads to the formation of cloud droplets. As the liquid-water clouds are radiatively opaque, this leads to the strongest cooling taking place at the cloud top (Pithan et al., 2014). The cloud-top cooling gives rise to turbulent mixing (Shupe et al., 2013; Brooks et al., 2017). Further cooling of the cloud gives rise to the formation of ice particles and thus the characteristic mixed-phase clouds observed during the cloudy state (Pithan et al., 2014). Despite the presence of ice particles making the ice-water mixture inherently unstable, these clouds are particularly persistent due to an interaction of micro-physical and dynamical processes (Morrison et al., 2012; Solomon et al., 2015). Eventually, all the liquid water in the cloud is lost by phase change and precipitation. The subsequent ice cloud is radiatively transparent and facilitates surface cooling leading to the formation of a surface-based inversion layer characteristic of the clear state (Pithan et al., 2014). Thus, air-mass transformation occurring during the transport of the air masses into the Arctic plays an important role in the formation of both the clear and the cloudy state.

The above-mentioned processes taking place during the air-mass transformation not only govern the formation of the two states but also govern the time scale and the spatial extent at which the transformation takes place. However, weather and climate models struggle to represent both the cloudy and clear state and their transformation in a Lagrangian framework (Pithan et al., 2016). This mismatch in representing the Arctic states results in substantial surface energy biases. Mixed-phase microphysics, specifically cloud phase partitioning and precipitation efficiency, as well as atmosphere-surface coupling, make an important contribution to the current model weaknesses (Klein et al., 2009; Morrison et al., 2012; Pithan et al., 2018).

Modelling air-mass transformations correctly is essential to capture air-mass transitions both temporally and spatially. Improving models will help to understand local-scale processes such as cloud microphysics and boundary-layer turbulence and their feedbacks on large-scale processes and coupling to the ocean and sea ice. This will, in turn, improve forecast capabilities in the Arctic and the mid-latitudes and projections of future Arctic climate change.

The observational basis for understanding the processes occurring during air-mass transformations has been developed through a Eulerian framework. However, air-mass transformations occur over Lagrangian pathways (Wexler, 2006; Curry, 1983; Emanuel, 2008; Brümmer, 1999; Pithan et al., 2018). Therefore, Pithan et al. (2018) suggest to follow an air mass which is advected into the Arctic and take observations along its path. Such repeated observations of individual air masses advected into the Arctic are currently lacking. The present study aims to address this knowledge gap, starting from the soundings taken during the Surface Heat Budget of the Arctic (SHEBA) experiment, computing air-mass back trajectories for these soundings, and compiling observations from the stations along the air-mass trajectory. Thus, we use the currently available Eulerian-based observations in a Lagrangian sense. Such an approach will provide observational snapshots of an air mass at different time intervals as it is advected polewards capturing different stages of the air-mass transformation. We focus on Arctic winter when the temperature contrasts between open ocean and sea ice provide a strong forcing for air-mass transformations.

2 | DATA AND METHODS

2.1 | Data

During the SHEBA expedition, an icebreaker was frozen into sea ice in the Beaufort Gyre from fall 1997 to summer 1998. Observations included a surface station measuring heat fluxes and standard meteorological variables on the sea

ice, and regular radiosondes as well as ground-based remote sensing instruments for cloud characterisation (Uttal et al., 2002). While the MOSAiC expedition in 2019/2020 targeted a transpolar drift in thin, largely first-year sea ice, the SHEBA domain in the late 1990ies was characterized by thick, multiyear sea-ice and the gyre circulation led to a smaller displacement of the drifting station (Dethloff et al., 2016).

Vaisala RS80-15GH radiosondes were deployed daily around 00:00 UTC and 12:00 UTC to measure temperature, humidity, and wind profiles at the SHEBA ice-camp site. However, the actual launch time of radiosondes varies slightly. We have used the quality-controlled version 2.0 of this dataset (Moritz, 2017). The air-mass transformation is depicted by compiling radiosonde observations from the Integrated Global Radiosonde Archive (IGRA) Version 2 (Durre et al., 2016) along the air-mass trajectories. The IGRA version 2 consists of radiosonde observations of temperature, humidity, and wind at stations across both Northern and Southern hemisphere and has been checked for quality assurance (Durre et al., 2006). Python code used to retrieve observations from a particular station and time in the IGRA archive can be downloaded from the GitHub repository (see Acknowledgments). A separate sounding dataset has been used for NY-Ålesund for one case study (Maturilli and Kayser, 2016). This dataset has been homogenized accounting for instrumentation errors and provides a higher vertical resolution compared to the corresponding profiles obtained from the IGRA.

Surface flux measurements were performed by the flux group tower at "Met City" in the SHEBA ice camp, which has been processed into hourly time series (Edgar et al., 2007). We have used the Net LW data from it. Cloud properties such as cloud base and cloud top are obtained from ETL Radar-Lidar Cloud Properties dataset, which combines cloud boundary information from both radar and lidar to obtain most accurate cloud base and top heights (Shupe et al., 2007).

2.2 | Generating Trajectories

Backward trajectories were calculated using the Hybrid Single-Particle Lagrangian Trajectory (HYSPLIT) Model of the National Oceanic and Atmospheric Administration (NOAA) Air Resources Laboratory (Stein et al., 2015). The trajectories were started at the actual launch time of the radiosondes using the coordinates of the soundings which vary due to the sea ice drift. They are computed at various heights corresponding approximately to standard pressure levels in the troposphere. The trajectories extend backwards in time for 5 days which is the typical time taken by an air mass to cross the Arctic (Woods and Caballero, 2016). The trajectory dataset can be downloaded from the PANGAEA archive (Ali and Pithan, 2019).

ERA-Interim reanalysis data (Berrisford et al., 2011) on a grid-scale of $0.75^\circ \times 0.75^\circ$ was used to drive the trajectory model. Wind speeds were extracted at 100, 200, 300, 400, 500, 600, 700, 800, 850, 925 and 1000 hPa at 6 hourly time steps. ERA-I offers a comparably high spatial resolution and performs better than other reanalysis products in the Arctic (Jakobson et al., 2012). It has also assimilated the observations from the SHEBA soundings. ECMWF's latest reanalysis product ERA-5 wasn't available at the time of performing this study. We have used Climate Data Record of Passive Microwave Sea Ice Concentration, Version 3 for plotting the sea ice concentration corresponding to the trajectories (Meier et al., 2017).

HYSPLIT offers various tools to study the consistency of the trajectories. We have verified the computational accuracy by starting the trajectories in the forward direction from the end-point of the backward trajectories. The spatial resolution of the meteorological data also affects the trajectories which was observed while using ERA-I on a grid-scale of $2.5^\circ \times 2.5^\circ$ for trajectory computation. Furthermore, the uncertainty associated with the centre point trajectory was estimated using HYSPLIT's standard meteorological grid offset ensemble configuration. In such a configuration, the meteorological data associated with each trajectory is offset 1 grid point in the horizontal and 0.01 sigma units in the vertical direction at the starting point. Only cases with small ensemble spread showing the robustness of the computed

trajectories were selected as case studies for this paper.

2.3 | Compiling Observations

The trajectories are sorted into the corresponding clear and cloudy states at SHEBA based on the Net LW criteria developed by Stramler et al. (2011). She defines a Net LW smaller than -30 Wm^{-2} as a clear state and, a Net LW greater than -10 Wm^{-2} as a cloudy state. The transition between clear and cloudy state can take place within hours (Stramler et al., 2011). We use a 3-hourly running mean of Net LW data to get more persistent states of the boundary layer.

Here, we focus our analysis on individual events as much of the moisture import into the Arctic Ocean occurs in a small number of moist intrusions (Woods et al., 2013; Liu and Barnes, 2015). The trajectories corresponding to lower levels of the troposphere at the SHEBA site, i.e; height above ground level (AGL) between 500-3000 m, are considered for capturing the transformation processes occurring in the lower atmosphere.

The challenges in compiling observations of air-mass transformation arise because of the sparse observation stations in the Arctic along with irregular daily time series. We have used a spatial threshold of 100 km for the air mass, i.e. a corresponding sounding is considered only if one of the trajectories passes at a distance of less than 100 km from the observation station. In most cases, the trajectories pass a station no more than six hours before or after a sounding has been taken. In one case (the station farthest from the SHEBA site for the 30th December 1998 case study) a sounding was lacking. The two adjacent soundings are approximately 12 hours apart from the time at which the air mass passed this station. Since both soundings show consistent air mass properties, we decided to interpolate temperature and humidities from both soundings to the time the air mass passed the station. Forward trajectories are generated from the SHEBA site for the cases in which we could capture observations from the backward trajectories.

Furthermore, it is important to note that the rationale behind this study is to capture the transformation in air masses which are advected in a reasonably barotropic manner as conceptualized with the help of the idealised model studies done before (Wexler, 1936; Curry, 1983; Emanuel, 2008; Pithan et al., 2014). This means that the trajectories at different vertical levels should be closely aligned spatially and temporally. There are several cases in which the air masses converge from different spatial sources into SHEBA (back-trajectories in Figure 8). It is extremely difficult to depict such cases solely with Lagrangian observations due to the strong shear involved. This constraint in air mass advection is monitored with the help of ensemble trajectories as described above. This rules out most of the cloudy-state intrusions taking place during December. Some aspects of air-mass transformation such as vertical velocities will be different in the presence of baroclinic disturbances. Yet, the remarkable consistency of observations of the cloudy state at the SHEBA site suggests that most air-mass transformations affect the temperature and humidity profiles in a similar way. Bearing in mind the role of vertical velocity, we therefore suggest that some generalisation of our results based on strictly barotropic cases is possible.

3 | RESULTS AND DISCUSSION

Sorting the 5-day back-trajectories based on the air mass state retrieved over the SHEBA site shows a clear distinction in air mass origin between clear and cloudy cases. Air masses that occupy the cloudy state over SHEBA predominantly have an origin or at least travelled over open ocean outside the Arctic, whereas air masses in the clear state have typically travelled over sea ice and continents in the five days prior to their arrival at SHEBA (Figure 2).

Moist air masses are more frequently advected from the Pacific than the Atlantic sector over SHEBA because of the expedition's location in the Beaufort Gyre. Over the entire Arctic basin, moist intrusions from the Atlantic play a

more dominant role (Woods and Caballero, 2016).

3.1 | Cloudy states caused by moist intrusions

The best observational coverage could be obtained for a moist intrusion beginning on 31st December 1997 and becoming evident at the SHEBA site in the 4th January 1998 23 UTC sounding. In this event, a strong meridional pressure gradient conducted warm, moist air into the Arctic, towards and around Greenland and to the SHEBA site as documented by Woods et al. (2013) (their Figure 1) using reanalysis data. The IR satellite images (Figure 4) reproduced from Persson et al. (2017) capture this warm and moist intrusion from the Fram Strait which is in agreement with our back-trajectories (blue dotted lines in Figure 3). Using these trajectories, we can match the air mass with soundings taken in the immediate vicinity of the ice edge and at the East coast of Greenland (Figure 3).

The temperature and moisture profiles obtained over open ocean and at the ice edge (Figure 5 A) show a moist, near-isobaric lower tropospheric structure similar to what has been assumed in idealized studies of air-mass transformations following moist intrusions (Wexler, 1936; Curry, 1983; Pithan et al., 2014). Observations of the air mass at the coast of Greenland, i.e. after it has travelled over sea ice for at least several hours, indicate substantial cooling and drying of the lower troposphere up to about 800 hPa. SHEBA cloud observations show a low-level cloud layer topping the boundary-layer and reaching into the temperature and moisture inversion (red and blue triangles in Figure 5 A show cloud top and base).

These observations support the conceptual view originally developed by Wexler (1936) that clouds deplete the lower troposphere of moisture as initially moist air masses are advected into the Arctic. While the near-surface air has cooled by more than 20 K in about three days, surface radiative cooling is small or absent when the air mass passes the SHEBA site ($\text{NetLW} \sim -5.5 \text{ W m}^{-2}$). The temperature structure shows a well-mixed boundary layer capped by a strong invigorated temperature inversion typical for the cloudy state of the boundary layer (Stramler et al., 2011). No matching observations were available for the forward trajectories for this case.

On 5th Jan, Persson et al. (2017) show the intrusion of drier and clear-sky air mass from the Canadian Archipelago into the SHEBA site which brings clear conditions at the SHEBA site. This is consistent with our back-trajectories (Figure 3) showing lower tropospheric levels intruding from Greenland and higher levels from the Canadian Arctic. The apparent contradiction between Persson et al. (2017) attributing the change from cloudy to clear skies at SHEBA to changes in the wind direction and Pithan et al. (2014) emphasizing the role of air-mass transformation from the cloudy to the clear state is merely a difference in perspective. From the Eulerian perspective of a (nearly) fixed observatory such as SHEBA, the change from cloudy to clear skies between January 4th and 5th is indeed caused by the advection of a different air-mass as shown by Persson et al. (2017). Meanwhile, the Lagrangian perspective adopted in the remainder of the present paper and in Wexler (1936); Curry (1983); Pithan et al. (2018) addresses what happens to an initially moist air mass both before and after it passes over the SHEBA site.

Our second case is based on an air mass arriving at the SHEBA site on January 10th (Figure 5 B). This air mass originated from the Siberian landmasses (brown trajectory lines in Figure 3) but crossed the open ocean before passing over Svalbard on its way to the SHEBA site. This moisture intrusion is also shown in a series of IR satellite images by Persson et al. (2017) (their Figure 4). The constant offset in temperatures in the mid-troposphere leads us to suspect that either or both sounding datasets may suffer from a temperature bias. Therefore, we focus our discussion on the shape of the profiles, which is not affected by such a temperature bias. The initial profiles over Russia show a strong near-surface temperature inversion, as we would expect for a continental polar air mass. When such air masses are advected over open ocean, they quickly pick up heat and moisture in a vigorously convective boundary layer (Pithan et al., 2018). This results in a substantially moister lower troposphere as the air mass passes over Svalbard (blue line in Figure 5 B). By the

time the air mass arrives over the SHEBA site, the near-surface layer has cooled and dried considerably.

On January 28th and February 27th, air masses from the Pacific ocean arrived at the SHEBA site. While these air masses would have been modified by uplift and descent when passing over the Alaskan Cordillera or Canadian Coast mountains, the profiles still show typical traces of the air-mass transformation expected from warm and moist air masses advected over sea ice such as elevated temperature and humidity inversion. We refrain from interpreting the temperature change, as the constant offset with height between SHEBA and the other soundings might point to a sensor issue.

3.2 | Clear states at SHEBA following the advection of cold, dry air masses

Cold and dry air masses with typical aspects of the clear boundary-layer state arrive at the SHEBA site on December 30th and January 12th. In both cases, the air masses come from the Siberian side, and at least the section of the back trajectories over the Arctic ocean has an anticyclonic curvature, in line with the observation that the clear state tends to be associated with anticyclonic conditions (Morrison et al., 2012) (Figure 6).

In both cases, the air masses are substantially colder and dryer at the SHEBA site than the air masses discussed above for the cloudy cases. Near-surface temperatures are around or below 240 K in both cases, and humidity is less than 1 gkg^{-1} throughout the troposphere. While upstream soundings are somewhat warmer and moister for the air mass reaching the SHEBA site on December 30th (Figure 7 A), they are substantially more moist for the air mass arriving at SHEBA on January 12th. This may be related to the fact that the trajectories for the first case come from far inland, whereas they originate closer to - and for one height level, over - the open ocean in the second case.

Besides confirming that air-mass origin plays a crucial role in determining the boundary-layer state in Arctic winter, these observations show that air masses continue to cool and dry after reaching the clear state, but qualitatively retain the temperature and moisture profiles characteristic of this boundary-layer state.

3.3 | Downstream transformation to the clear state

Forward, i.e. downstream trajectories from SHEBA allowed us to match observations of air mass development after the air mass passed over the SHEBA site in one additional case (Figure 8). Over SHEBA, the air mass is already rather dry and cold, but still in the cloudy state ($\text{NetLW} \sim -9.6 \text{ W m}^{-2}$). While the downstream sounding one day later shows similar air-mass properties and even slightly warmer and moister conditions around 800 hPa, the sounding four days after the air mass has passed over the SHEBA site shows a substantially colder and dryer air mass.

While the cooling and drying of the air mass after a moist intrusion is initially confined to the lower troposphere and profiles remain largely unchanged above 750 to 800 hPa (Figure 5), this example shows how the cooling and drying eventually extend further up throughout the troposphere. This likely involves other processes than the canonical development of Arctic stratus clouds capping the boundary layer. Which processes control the mid-tropospheric drying and cooling remains to be investigated. Downstream observations for the other cloudy state cases shown in Figure 3 could not be compiled as their trajectories diverge downstream of SHEBA.

4 | SUMMARY AND CONCLUSIONS

Backward trajectories for the radiosondes launched during DJF in the icebreaker campaign SHEBA in the Beaufort Gyre show that the cloudy state of the boundary layer (Stramler et al., 2011) is usually associated with a marine air-mass

origin, whereas the clear state is tied to a continental air mass source. Comparing SHEBA and upstream soundings for selected barotropic events shows how the initially warm and moist air masses cool and dry once they are advected over sea ice. The boundary layer is most affected by the cooling and drying, which creates the temperature and humidity inversions often found over the Arctic throughout the year. In one case, an air mass originating over the continent passes over open ocean before reaching the ice edge, rapidly picking up moisture on the way.

Compiling local observations into a Lagrangian, air-mass following framework, we have created the first direct observational evidence of air-mass transformations creating the cloudy and clear states of the Arctic boundary-layer (Pithan et al., 2018). We recommend the use of this approach for other past, ongoing and future campaigns.

We have compiled a set of case studies where SHEBA soundings can be compared to upstream and in one case downstream soundings. We recommend using these cases for future single-column model or Large-Eddy Simulation studies to go beyond the highly idealized studies that have been conducted in the past (Pithan et al., 2016).

4.0.1 | Supporting Information

Supporting information provides the link to the repository which hosts the code for generating the figures used in this study.

ACKNOWLEDGEMENTS

We would like to acknowledge Helmholtz postdoc project "Understanding the role of atmosphere surface coupling for large-scale dynamics", the SHEBA data-sets (Moritz, 2017; Edgar et al., 2007; Shupe et al., 2007) and the HYSPLIT software tool (Stein et al., 2015) which made this work possible. ERA-I (Berrisford et al., 2011), sea ice concentration data (Meier et al., 2017), and open-source Python packages helped us immensely to conduct this research (McKinney et al., 2010; Hunter, 2007; May et al., 2008 - 2020; Hoyer and Hamman, 2017). We would also like to extend our gratitude to Thomas Jung for his constant support in carrying out this project and to two anonymous reviewers whose comments have helped us to improve the manuscript. The code used for producing the figures is available at https://github.com/avatar101/project_SHEBA.

CONFLICT OF INTEREST

The authors declare no conflict of interest.

ENDNOTES

REFERENCES

- Albritton, S. M. and Pithan, F. (2019) Backwards and forward trajectory data for wintertime (DJF) corresponding to Surface Heat Budget of the Arctic (SHEBA) expedition. doi:10.1594/PANGAEA.899851.
- Bennartz, R., Shupe, M., Turner, D., Walden, V., Steffen, K., Cox, C., Kulie, M., Miller, N. and Pettersen, C. (2013) July 2012 Greenland melt extent enhanced by low-level liquid clouds. *Nature*, **496**, 83.
- Berrisford, P., Dee, D., Poli, P., Brugge, R., Fielding, K., Fuentes, M., Kallberg, P., Kobayashi, S., Uppala, S. and Simmons, A. (2011) The ERA-Interim archive version 2.0, ERA report series 1, ECMWF, Shinfield Park. *Reading, UK*, **13177**.

- Brooks, I. M., Tjernström, M., Persson, P. O. G., Shupe, M. D., Atkinson, R. A., Canut, G., Birch, C. E., Mauritsen, T., Sedlar, J. and Brooks, B. J. (2017) The Turbulent Structure of the Arctic Summer Boundary Layer During The Arctic Summer Cloud-Ocean Study. *Journal of Geophysical Research: Atmospheres*, **122**, 9685–9704.
- Brümmer, B. (1999) Roll and cell convection in wintertime arctic cold-air outbreaks. *Journal of the Atmospheric Sciences*, **56**, 2613–2636.
- Cohen, L., Hudson, S. R., Walden, V. P., Graham, R. M. and Granskog, M. A. (2017) Meteorological conditions in a thinner Arctic sea ice regime from winter to summer during the Norwegian Young Sea Ice expedition (N-ICE2015). *Journal of Geophysical Research: Atmospheres*, **122**, 7235–7259.
- Curry, J. (1983) On the formation of continental polar air. *Journal of the Atmospheric Sciences*, **40**, 2278–2292.
- Dettlaff, K., Rex, M. and Shupe, M. (2016) Multidisciplinary Drifting Observatory for the Study of Arctic Climate (MOSAIC). *Journal of Geophysical Research: Atmospheres*, **121**, 3064.
- Doyle, J., Lesins, G., Thackray, C., Perro, C., Nott, G., Duck, T., Damoah, R. and Drummond, J. (2011) Water vapor intrusions into the High Arctic during winter. *Geophysical Research Letters*, **38**.
- Durre, I., Vose, R. S. and Wuertz, D. B. (2006) Overview of the integrated global radiosonde archive. *Journal of Climate*, **19**, 53–68.
- Durre, I., Xungang, Y., Vose, S. R., Applequist, S. and Arnfield, J. (2016) Integrated Global Radiosonde Archive (IGRA), Version 1.0. NOAA National Centers for Environmental Information. Accessed 16 Nov 2017. doi:10.7289/V5X63K0Q.
- Edgar, A., Fairall, C., Guest, P. and Persson, O. (2007) Tower, 5-level hourly measurements plus radiometer and surface flux data at Met City (ASFG). Version 1.0 [Data set]. UCAR/NCAR - Earth Observing Laboratory. Accessed 16 nov 2017. doi:10.5065/D65H7DNS.
- Emanuel, K. (2008) Back to Norway: an essay. *Meteorological Monographs*, 87–96.
- Graham, R. M., Rinke, A., Cohen, L., Hudson, S. R., Walden, V. P., Granskog, M. A., Dorn, W., Kayser, M. and Maturilli, M. (2017) A comparison of the two arctic atmospheric winter states observed during N-ICE2015 and SHEBA. *Journal of Geophysical Research: Atmospheres*, **122**, 5716–5737.
- Granskog, M. A., Assmy, P., Gerland, S., Spreen, G., Steen, H. and Smedsrud, L. H. (2016) Arctic research on thin ice: Consequences of Arctic sea ice loss. *Eos Trans. AGU*, **97**, 22–26.
- Hansen, J., Ruedy, R., Sato, M. and Lo, K. (2010) Global surface temperature change. *Reviews of Geophysics*, **48**.
- Hammer, S. and Hamman, J. (2017) xarray: N-D labeled arrays and datasets in Python. *Journal of Open Research Software*, **5**. doi:10.5334/jors.148.
- Hunter, J. D. (2007) Matplotlib: A 2D graphics environment. *Computing In Science & Engineering*, **9**, 90–95. doi:10.1109/MCSE.2007.55.
- Jakobson, E., Vihma, T., Palo, T., Jakobson, L., Keernik, H. and Jaagus, J. (2012) Validation of atmospheric reanalyses over the central Arctic Ocean. *Geophysical Research Letters*, **39**.
- Johansson, E., Devasthale, A., Tjernström, M., Ekman, A. M. and L'Ecuyer, T. (2017) Response of the lower troposphere to moisture intrusions into the Arctic. *Geophysical Research Letters*, **44**, 2527–2536.
- Jung, T., Gordon, N. D., Bauer, P., Bromwich, D. H., Chevallier, M., Day, J. J., Dawson, J., Doblus-Reyes, F., Fairall, C., Goessling, H. F. et al. (2016) Advancing polar prediction capabilities on daily to seasonal time scales. *Bulletin of the American Meteorological Society*, **97**, 1631–1647.

- Jung, T., Kasper, M. A., Semmler, T. and Serrar, S. (2014) Arctic influence on subseasonal midlatitude prediction. *Geophysical Research Letters*, **41**, 3676–3680.
- Kapsch, M.-L., Graverson, R. G. and Tjernström, M. (2013) Springtime atmospheric energy transport and the control of Arctic summer sea-ice extent. *Nature Climate Change*, **3**, 744.
- Kapsch, M.-L., Graverson, R. G., Tjernström, M. and Bintanja, R. (2016) The Effect of Downwelling Longwave and Shortwave Radiation on Arctic Summer Sea Ice. *Journal of Climate*, **29**, 1143–1159. doi:10.1175/JCLI-D-15-0238.1.
- Klein, S. A., McCoy, R. B., Morrison, H., Ackerman, A. S., Avramov, A., Boer, G. d., Chen, M., Cole, J. N., Del Genio, A. D., Falk, M. et al. (2009) Intercomparison of model simulations of mixed-phase clouds observed during the arm mixed-phase arctic cloud experiment. i: Single-layer cloud. *Quarterly Journal of the Royal Meteorological Society: A Journal of the Atmospheric Sciences, Applied Meteorology and Physical Oceanography*, **135**, 979–1002.
- Liu, C. and Barnes, E. A. (2015) Extreme moisture transport into the Arctic linked to Rossby wave breaking. *Journal of Geophysical Research: Atmospheres*, **120**, 3774–3788.
- Maturilli, M. and Kayser, M. (2016) Homogenized radiosonde record at station Ny-Ålesund, Spitsbergen in 1998. PANGAEA. In supplement to: Maturilli, M.; Kayser, M (2016): Arctic warming, moisture increase and circulation changes observed in the Ny-Ålesund homogenized radiosonde record. Theoretical and Applied Climatology, 17 pp, doi:10.1007/s00704-016-864-0.
- May, R., Arms, S., Marsh, P., Bruning, E. and Leeman, J. (2008 - 2020) Metpy: A Python package for meteorological data. doi:10.5065/D6WW7G29.
- McKinney, W. et al. (2010) Data structures for statistical computing in Python. In *Proceedings of the 9th Python in Science Conference*, vol. 445, 51–56. Austin, TX.
- Meier, W., Fetterer, F., Savoie, M., Mallory, S., Duerr, R. and Stroeve, J. (2017) NOAA/NSIDC Climate Data Record of Passive Microwave Sea Ice Concentration, Version 3. Boulder, Colorado USA. NSIDC: National Snow and Ice Data Center. Accessed 16 Nov 2017. doi:10.7265/N59P2ZTG.
- Mertz, R. (2017) Soundings, Ice Camp NCAR/GLAS raobs. (ASCII). Version 2.0. UCAR/NCAR - Earth Observing Laboratory. Accessed 01 Oct 2017. doi:10.5065/D6FQ9V0Z.
- Morrison, H., De Boer, G., Feingold, G., Harrington, J., Shupe, M. D. and Sulia, K. (2012) Resilience of persistent Arctic mixed-phase clouds. *Nature Geoscience*, **5**, 11.
- Murphy, M., Svensson, G., Graverson, R. G., Kapsch, M.-L., Stroeve, J. C. and Boisvert, L. N. (2016) Melt onset over Arctic sea ice controlled by atmospheric moisture transport. *Geophysical Research Letters*, **43**, 6636–6642.
- Parish, D.-S. R., Lee, S. and Feldstein, S. B. (2015) Attribution of the recent winter sea ice decline over the Atlantic sector of the Arctic Ocean. *Journal of climate*, **28**, 4027–4033.
- Perovich, P. O. G., Fairall, C. W., Andreas, E. L., Guest, P. S. and Perovich, D. K. (2002) Measurements near the Atmospheric Surface Flux Group tower at SHEBA: Near-surface conditions and surface energy budget. *Journal of Geophysical Research: Oceans*, **107**, SHE-21.
- Perovich, P. O. G., Shupe, M. D., Perovich, D. and Solomon, A. (2017) Linking atmospheric synoptic transport, cloud phase, surface energy fluxes, and sea-ice growth: Observations of midwinter SHEBA conditions. *Climate Dynamics*, **49**, 1341–1364.
- Pithan, F., Ackerman, A., Angevine, W. M., Hartung, K., Ickes, L., Kelley, M., Medeiros, B., Sandu, I., Steeneveld, G.-J., Sterk, H. et al. (2016) Select strengths and biases of models in representing the Arctic winter boundary layer over sea ice: the Marcform 1 single column model intercomparison. *Journal of Advances in Modeling Earth Systems*, **8**, 1345–1357.
- Pithan, F., Medeiros, B. and Mauritsen, T. (2014) Mixed-phase clouds cause climate model biases in Arctic wintertime temperature inversions. *Climate Dynamics*, **43**, 289–303.

Pithan, F., Svensson, G., Caballero, R., Chechin, D., Cronin, T. W., Ekman, A. M., Neggers, R., Shupe, M. D., Solomon, A., Tjernström, M. et al. (2018) Role of air-mass transformations in exchange between the Arctic and mid-latitudes. *Nature Geoscience*, **11**, 805.

Serreze, M. C., Barrett, A. P., Slater, A. G., Steele, M., Zhang, J. and Trenberth, K. E. (2007) The large-scale energy budget of the Arctic. *Journal of Geophysical Research: Atmospheres*, **112**.

Shupe, M., Intrieri, J. and Uttal, T. (2007) ETL Radar-Lidar 10-min Cloud Physical Properties. Version 1.0. UCAR/NCAR - Earth Observing Laboratory. Accessed 02 May 2018. doi:10.5065/d6ms3r4g.

Shupe, M., Persson, P., Brooks, I., Tjernström, M., Sedlar, J., Mauritsen, T., Sjogren, S., Leck, C. et al. (2013) Cloud and boundary layer interactions over the Arctic sea ice in late summer. *Atmos. Chem. Phys.*, **13**, 9379–9399.

Solomon, A., Feingold, G. and Shupe, M. (2015) The role of ice nuclei recycling in the maintenance of cloud ice in arctic mixed-phase stratocumulus. *Atmospheric Chemistry and Physics*, **15**, 10631–10643. doi:10.5194/acp-15-10631-2015.

Stern, A., Draxler, R. R., Rolph, G. D., Stunder, B. J., Cohen, M. and Ngan, F. (2015) NOAA's HYSPLIT atmospheric transport and dispersion modeling system. *Bulletin of the American Meteorological Society*, **96**, 2059–2077.

Stranler, K., Del Genio, A. D. and Rossow, W. B. (2011) Synoptically driven Arctic winter states. *Journal of Climate*, **24**, 1747–1762.

Uttal, T., Curry, J. A., McPhee, M. G., Perovich, D. K., Moritz, R. E., Maslanik, J. A., Guest, P. S., Stern, H. L., Moore, J. A., Turenne, R. et al. (2002) Surface heat budget of the Arctic Ocean. *Bulletin of the American Meteorological Society*, **83**, 255–276.

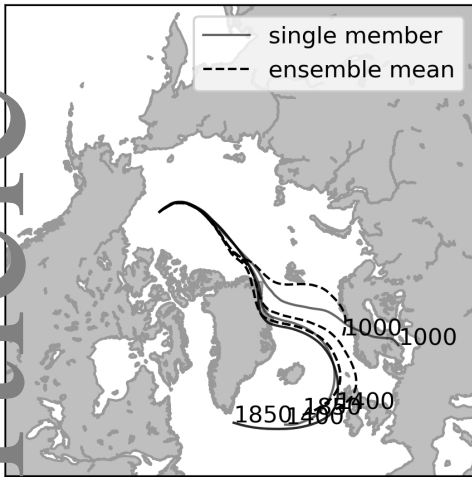
Walter, B. A., Overland, J. E. and Turet, P. (1995) A comparison of satellite-derived and aircraft-measured regional surface sensible heat fluxes over the beaufort sea. *Journal of Geophysical Research: Oceans*, **100**, 4585–4591.

Wexler, H. (1936) Cooling in the lower atmosphere and the structure of polar continental air. *Mon. Wea. Rev.*, **64**, 122–136.

Woods, C. and Caballero, R. (2016) The role of moist intrusions in winter Arctic warming and sea ice decline. *Journal of Climate*, **29**, 4473–4485.

Woods, C., Caballero, R. and Svensson, G. (2013) Large-scale circulation associated with moisture intrusions into the Arctic during winter. *Geophysical Research Letters*, **40**, 4717–4721.

(a) 4 Jan 1998 23 UTC



(b) 5 Jan 1998 23 UTC

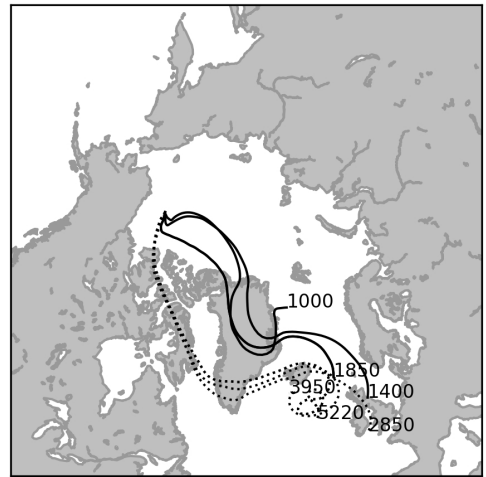
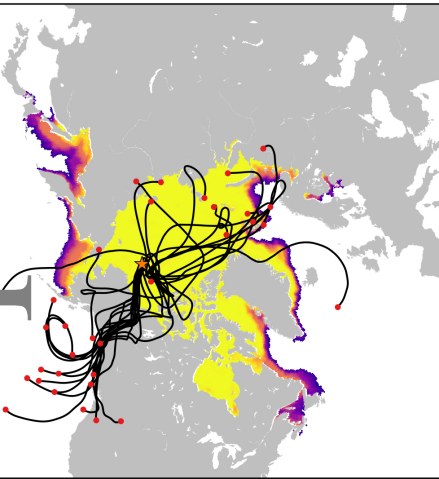


FIGURE 1 (a) back trajectory computations for ensemble mean vs single member for 4th Jan which are spatially confined (b) back trajectories for 5th Jan where upper tropospheric levels (dotted lines) diverge from lower levels (solid lines).

Cloudy



Clear

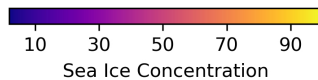
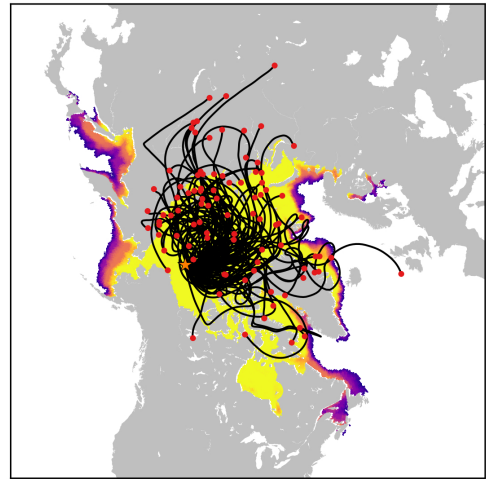


FIGURE 2 5-day back trajectories starting at 1400 m for the cloudy (left) and clear (right) cases observed at the SHEBA site during DJF. Background colour shows the mean sea ice concentration for SHEBA DJF (Meier et al., 2017)

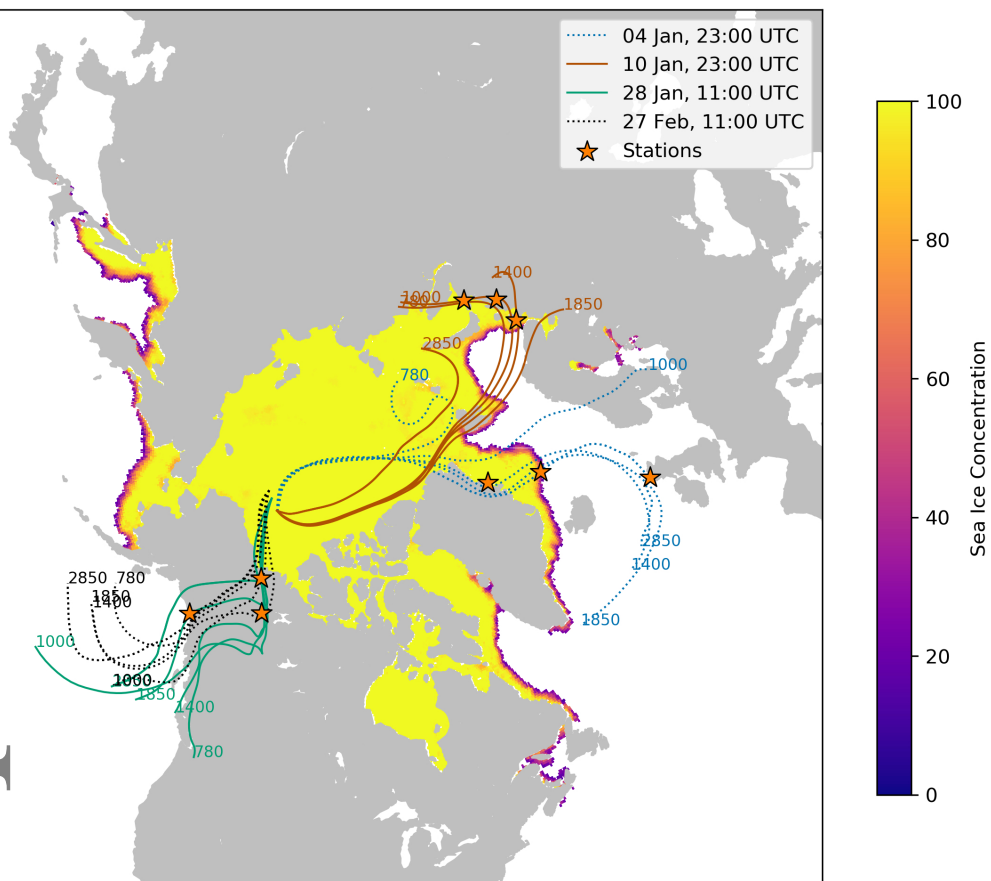


FIGURE 3 Back trajectories for the cloudy case studies discussed in this paper at 780 m, 1000 m, 1400 m, 1850 m, 2850 m above ground level, along with sounding stations depicted by yellow stars.

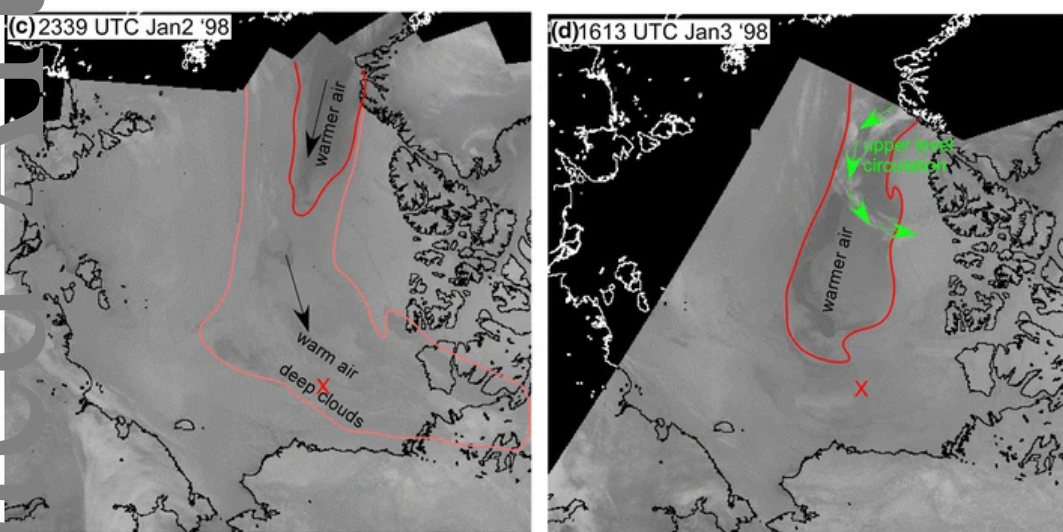


FIGURE 4 IR Satellite images corresponding to Jan 4 1998 case showing the intrusion of warm and moist air from Fram Strait captured by NOAA's polar orbiting satellite, figure reproduced from Persson et al. (2017, Figure 1)

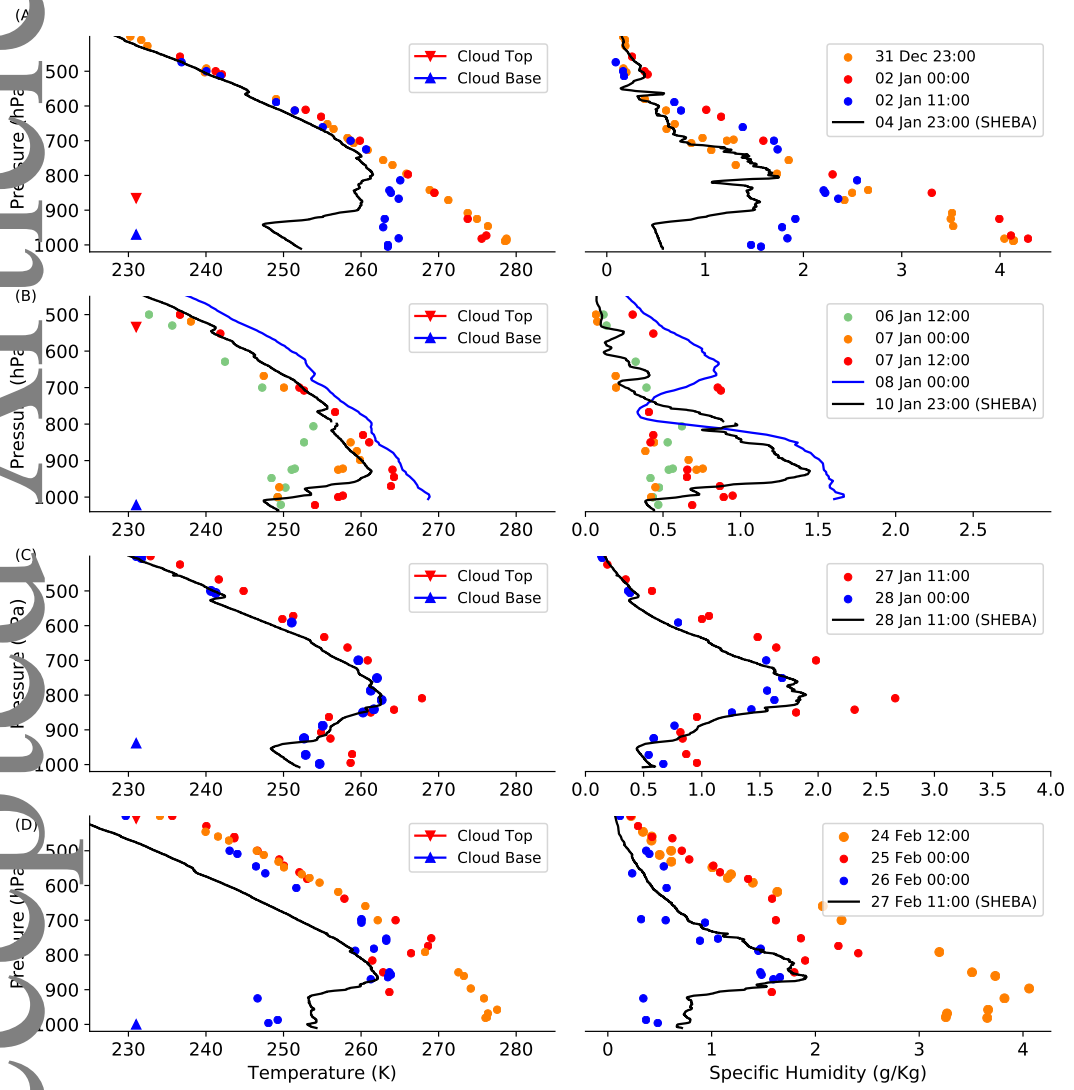


FIGURE 5 Observed profiles of temperature and humidity for cloudy state cases at the SHEBA site. Circles show observations from upstream sounding stations matching the corresponding air-mass trajectory.

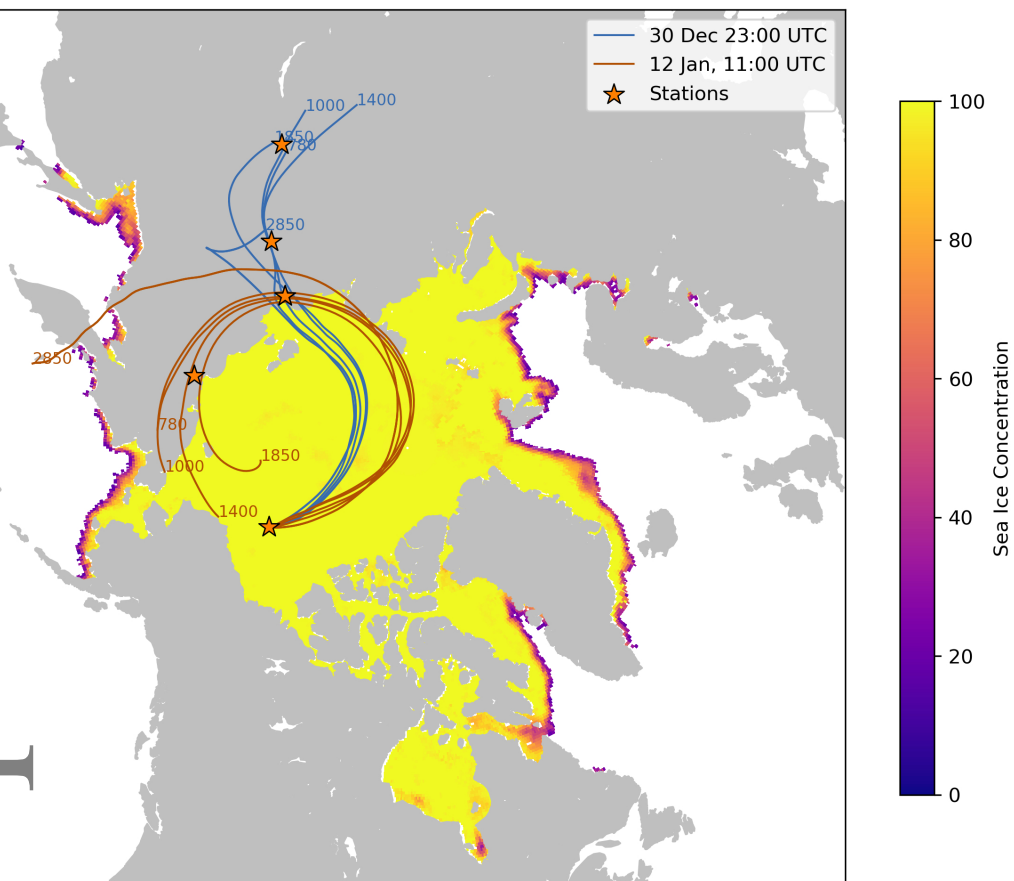


FIGURE 6 Back trajectories for selected clear boundary-layer states at SHEBA levels 780 m, 1000 m, 1400 m, 1850 m, 2850 m above ground, along with sounding stations depicted by yellow stars.

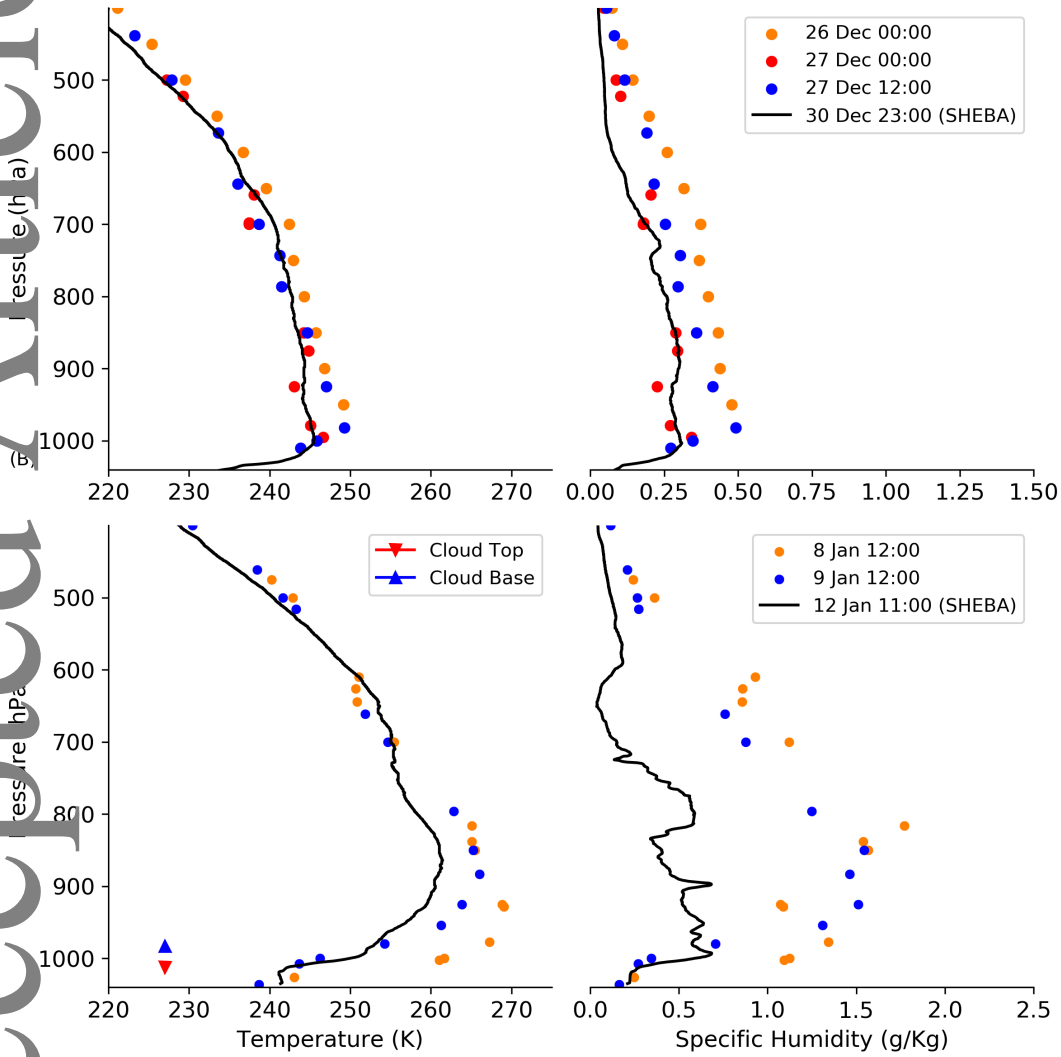


FIGURE 7 Observed profiles of temperature and humidity for clear state cases at the SHEBA site. Circles show observations from upstream sounding stations matching the corresponding air-mass trajectory.

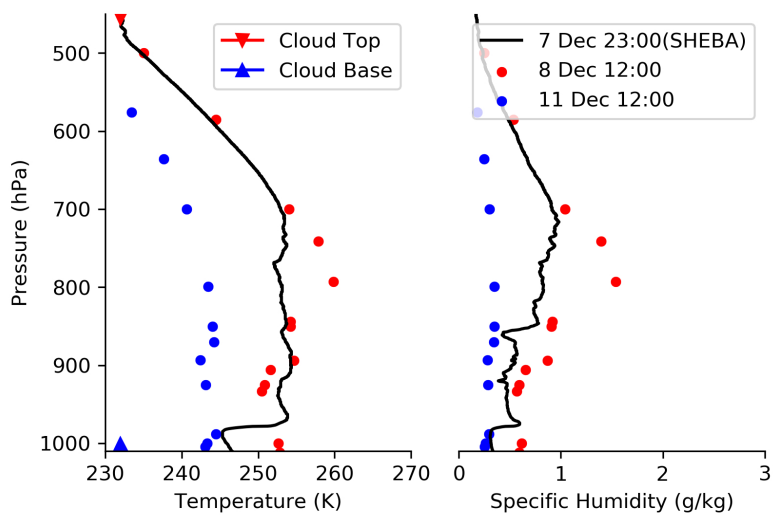
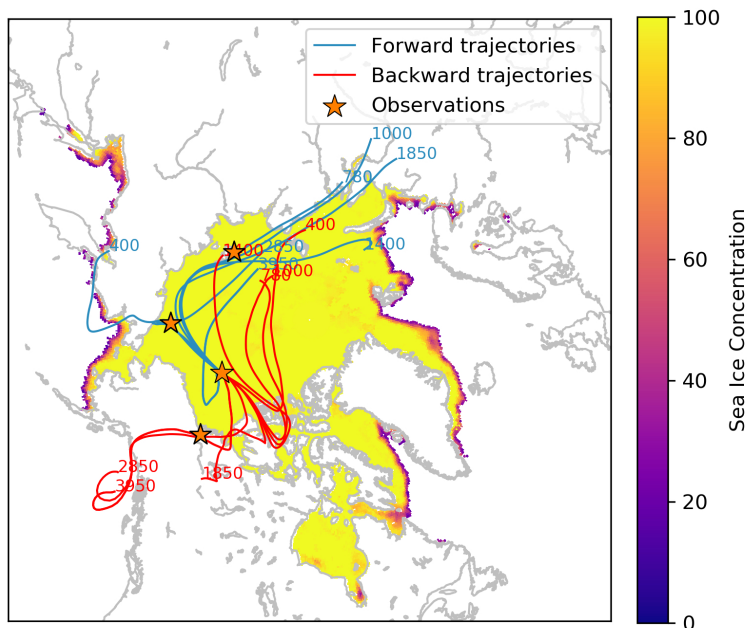


FIGURE 8 Forward and backward trajectories starting 7th December over the SHEBA site and matching soundings. No soundings were available for the upstream station shown in the map.